

High-throughput Virtual Screening- and Molecular Docking-based Prediction for Acetylcholinesterase Inhibitors and Exploring its Mechanisms against Alzheimer's Disease based on Network Pharmacology

Pitchayakarn Takomthong¹, Pornthip Waiwut², Carlo Ballatore³, Kiattawee Choowongkomon⁴, Pughu Novi Arsito⁵, Yaowared Chulikhit¹ and Chantana Boonyarat^{1,6}

¹Faculty of Pharmaceutical Sciences, Khon Kaen University, Khon Kaen, ²Faculty of Pharmaceutical Sciences, Ubon Ratchathani University, Ubon Ratchathani, Thailand, ³Skaggs School of Pharmacy and Pharmaceutical Sciences, University of California, San Diego, Gilman Drive, La Jolla, California, United States, ⁴Department of Biochemistry, Faculty of Science, Kasetsart University, Bangkok, Thailand, ⁵School of Pharmacy, Faculty of Medicine and Health Sciences, Universitas Muhammadiyah Yogyakarta, Yogyakarta, Indonesia, ⁶Protein and Proteomics Research Center for Commercial and Industrial Purposes, Faculty of Science, Khon Kaen University, Khon Kaen, Thailand

Correspondence:

Chantana Boonyarat, PhD,
Faculty of Pharmaceutical
Sciences, Khon Kaen University,
123 Moo 16 Mitraphab Road,
Muang, Khon Kaen 40002,
Thailand.
e-mail: chaboo@kku.ac.th

Received: March 23, 2024;

Revised: April 24, 2024;

Accepted: May 3, 2024

ABSTRACT

OBJECTIVE This study aimed to identify promising ligands for inhibiting acetylcholinesterase (AChE) activity using virtual screening (VS).

METHODS VS was used to identify potential AChE inhibitors from the PubChem database. Ligands with favorable binding pocket interactions were selected. SwissADME and pkCSM tools were used to assess drug-likeness and pharmacokinetic properties. Molecular dynamic (MD) simulations provided insights into binding interactions. Network pharmacology was used to explore interactions between the target molecule and AD-related genes to determine its mechanism of action.

RESULTS VS identified promising AChE inhibitor candidates with acridone, carbazole, and xanthone scaffolds. Docking simulations showed strong binding with AChE. These ligands displayed favorable drug-likeness and ADMET properties, with one (M5) lacking predicted hepatotoxicity. MD simulations suggested stable binding of M5 to AChE, potentially affecting both catalytic and peripheral sites, hinting at dual inhibition. M5's interactions, especially near His440, appeared more favorable than donepezil. Network analysis implicated M5 in targeting multiple pathways in AD, with potential focus on neuroinflammation.

CONCLUSIONS This study identified promising AChE inhibitor candidates through virtual screening. Ligand M5 emerged as particularly promising due to its favorable binding characteristics, lack of predicted hepatotoxicity, and potential for targeting multiple pathways in AD. However, further *in vitro* and *in vivo* validation is essential for clinical development.

KEYWORDS virtual screening, acetylcholinesterase inhibitors, PubChem database, molecular dynamics simulation, gene ontology, KEGG pathways

© The Author(s) 2024. Open Access



This article is licensed under a Creative Commons Attribution 4.0 International License, which permits use, sharing, adaptation, distribution and reproduction in any medium or format, as long as you give appropriate credit to the original author(s) and the source, provide a link to the Creative Commons licence, and indicate if changes were made.

INTRODUCTION

Alzheimer's disease is a progressive neurological disorder characterized by cognitive decline. It is an age-related disease and the most common

cause of dementia among the elderly (1). The AD neuropathological hallmark is the accumulation of amyloid beta (A β) plaques and neurofibrillary tangles. However, some studies have reported

pathophysiological changes during the AD progression involving the depletion of acetylcholine (ACh) neurotransmitter as well as oxidative stress and neuroinflammation. ACh is regulated by the cholinergic system, playing a crucial role in memory and learning processes. Its activity is modulated by acetylcholinesterase (AChE), which also terminates its function (2). The loss of cholinergic neurotransmission is responsible for deterioration of cognitive function observed in the AD brain (3). Treatment with AChE inhibitors (AChEIs) has been shown to be associated with a slower cognitive decline (4), and it is currently used as a main approach for AD treatment in mild and moderate stages (5). There are still challenges in AD drug discovery because no novel anti-AD drugs have been approved for years. Although aducanumab received accelerated approval from the USFDA in June 2021, experts continue to discuss arguments in favor of aducanumab due to insufficiency of evidence supporting its ability to prevent or reverse the AD symptoms (6).

Virtual screening (VS), a pivotal initial step in rational drug design, involves computationally screening large libraries of chemical compounds to identify potential drug candidates that could interact with a specific target of interest (7, 8). It is possible to interpret and screen millions of ligands in a matter of minutes, resulting in the identification of novel chemical structures with great potential for pharmacological activity (9). Additionally, computational approaches can predict physical, chemical, and pharmacokinetic properties to assess the potential drug candidate based on the structure of a ligand (10). Molecular dynamics (MD) simulations complement virtual screening by providing insights into the dynamic behavior of biomolecular systems at the atomic level, elucidating protein-ligand interactions and conformational changes over time (11). Integrated with network pharmacology, it has the capacity to comprehensively analyze complex interactions between drugs, targets, and biological pathways within a network framework. Together, these techniques offer a powerful synergistic approach to drug discovery, facilitating the rational design of novel therapeutics and the exploration of their pharmacological mechanisms of action.

To overcome the challenges of AD, one of the approaches to developing ligands based on tacrine-

scaffold with anti-AChE activity is particularly fascinating because the presence of condensed aromatic cores in tacrine contributes to high ligand efficiency. In this study, we utilized VS to screen planar aromatic ligands from PubChem that could potentially act as AChEIs. These ligands were then visually inspected, and their binding poses in the AChE binding pocket were analyzed. Promising ligands were subjected to further screening for drug likeness and ADMET properties using SwissADME (12) and pkCSM (13) online webserver. In combination with MD, we studied the binding interactions between molecules to provide insights into the biomolecular processes and function. Additionally, network pharmacology has been utilized to study the complex interactions between M5 and gene targets related to AD with the objective of understanding its predicted mechanism of action.

METHODS

Enzyme template validation

Over 2500 x-ray AChE crystal structures were obtained from PDB. The AChE templates were superimposed one by one to confirm the position of the active site. All ligands in each template were extracted and their energies minimized before performing molecular docking. Water was deleted from each template, hydrogen atoms were added, and charges were assigned for template preparation. Re- and cross-docking were performed as a validation procedure and the results were analyzed using root mean squared deviation (RMSD) between the docked pose and the former crystal conformer.

Molecular docking and post-docking analysis

High-throughput docking-based virtual screening was performed using the GOLD program version 5.3.0. The semi-empirical ChemPLP scoring function was used to validate the ligand binding modes and obtain the relative binding energy. The active site was identified following treatment with donepezil which is one of the first-line AChEIs for AD treatment. Ten docking runs per ligand were conducted for pilot virtual screening. In the post-docking process, Autodock 4.2.6 was used to observe the binding interaction of the top-ranked ligands. To elucidate the binding interaction, hits were docked in the AChE active site using Lamarckian generic algorithms. A grid map (70 Å

x 70 Å x 70 Å) with 0.375 Å of grid spacing, and a default box size of x=4.753 Å, y=66.521 Å, z= 64.857 Å was generated to cover the active site. Discovery studio 2020 was used for depth analysis of the ligand-AChE complexes.

Physiochemical properties and pharmacokinetic prediction

SwissADME and pKCSM were utilized in this study to evaluate the physicochemical properties and the pharmacokinetics of potential drug candidates. The absorption factor was evaluated based on intestinal absorption, while the volume of distribution (VDss) was used to determine whether the drug was primarily distributed in the plasma or tissues. In addition, the blood-brain barrier (BBB) permeability (logBB) and central nervous system (CNS) permeability were used to assess brain distribution. The CYP450 inhibition model was used to predict metabolism, while renal OCT2 substrate was used to predict excretion. Finally, the hepatotoxicity was predicted to evaluate drug toxicity.

Molecular dynamics (MD) simulation

The molecular dynamics (MD) simulation was carried out with OpenMM using Google Compute Engine backend (GPU) Python 3; the GPU nodes assigned are NVIDIA-SMI 525.85.12, Driver Version 525.85.12, and CUDA Version 12.0 (14). ff19SB and GAFF2 force fields from AMBER tools were used to minimize the bond stretching energy of protein and ligand, respectively (15). The TIP3P water model produced and solvated apo AChE (unbound), the AChE-ligand complex, and the AChE-donepezil complex before neutralizing them with NaCl ions. Before running the MD simulation, its concentration was set to 0.15 M. The 50 ns MD simulations were performed under constant temperature (310 K) and pressure (1 bar) after reaching equilibrium. The frequency of trajectory file was written and set to 10 ps. Structural stability, flexibility, and compactness were analyzed from root mean square deviation (RMSD), root mean square fluctuation (RMSF), and the radius of gyration (RoG), respectively.

The protein-protein interaction (PPI) network, clustering and functional enrichment analysis

SwissTargetPrediction and GeneCards were used to identify predicted target genes of hit and

AD, respectively. The common target prediction between hit and AD was generated by Venn diagram. To establish the protein-protein interaction (PPI) network, STRING database was used and the minimum interaction threshold was set as medium confidence (>0.4) with “*Homo sapiens*” species. The shared target of hit and AD were imported into ShinyGO V0.77 to analyze Gene Ontology (GO) enrichment and KEGG pathways. The top 10 targets were constructed and were then clustered using kmeans from the String global scores.

RESULTS

AChE template preparation and validation

From 2,500 templates, 24 TcAChE structures with similar folds were identified. Resolution ranged from 2.05 to 2.85 Å, with 2CEK (2.01 Å) being the most favorable. Re-docking and cross-docking validations (Figure 1) suggested 2CEK's superior ability to accommodate diverse ligands with good accuracy (low RMSD), making it ideal for docking simulations. Therefore, 2CEK was chosen for further docking studies.

High-throughput virtual screening for AChE inhibitors

Following the workflow outlined in Figure 2A, a high-throughput virtual screening based on docking simulations was conducted to identify potential AChE inhibitors. Seven ligand classes (17,330 ligands) were selected for analysis, including phenothiazine, phenoxazine, phenazine, acridone, acridine, xanthone, and carbazole (Figure 2B). These ligands were virtually screened and docked within the binding pocket of AChE using the GOLD program. Ligands exhibiting a docking score superior to donepezil (93.01 kcal/mol) were predicted to bind potently with AChE. The remaining 388 ligands displayed scores ranging from 93.02 to 124.04 kcal/mol. Lipinski's rule (16) was applied to assess the drug-likeness of these ligands, considering their potential as oral drug candidates. This analysis identified 32 ligands for further investigation of their in-silico blood-brain barrier (BBB) permeability using SwissADME. Ultimately, eight ligands were identified as capable of crossing the BBB. These promising candidates included three acridones, one acridine, two carbazoles, and two xanthenes.

PDB ID / Ligand	1H22_E20	1UT6_A6N	2CEK_N8T	2CMF_F11	2ACK_EDR	3I6M_G3X	3I6Z_G6X	1E3Q_EBW	1EVE_E20	1E66_HUX	2W6C_BM4	1DX6_GNT	1W6R_GNT	1GPK_HUP	Mean RMSD
1H22	1.82	4.41	3.34	2.15	3.28	2.4	2.63	2.66	1.61	6.91	2.93	0.37	0.55	0.71	2.56
1H23	1.97	4.39	3.38	1.99	3.05	4.71	2.62	2.81	1.7	7.53	1.7	0.57	0.54	0.77	2.70
1ODC	2.75	2.22	2.84	1.34	5.12	5.38	3.04	2.99	2.43	1.15	1.78	0.68	0.98	1.81	2.47
1UT6	1.5	1.27	3.51	0.99	3.68	4.77	2.84	2.77	4.73	1.03	1.68	0.62	0.98	0.76	2.22
1ZGB	2.69	1.84	3.03	1.85	5.45	4.7	3.66	2.85	1.82	0.93	1.81	0.57	0.66	0.63	2.32
2CEK	0.88	1.45	1.37	2.07	5.57	1.02	3.6	2.1	3.02	0.99	1.13	0.6	0.73	3.59	2.01
2CKM	2.87	2.13	2.64	0.97	4.55	4.66	3.03	2.84	3.8	0.7	1.23	0.36	0.55	1.78	2.29
2CMF	3.77	1.26	2.9	0.65	6.91	4.68	4.04	2.69	2.71	0.59	5.36	3.87	3.54	2.02	3.21
2ACK	2.42	5.15	3.25	2.27	0.77	4.91	3.07	2.27	3.24	3.68	5.36	1.09	1.01	1.98	2.89
3I6M	2.72	4.08	2.97	2.54	4.16	0.62	1.71	3.33	1.74	7.1	3.1	0.73	0.81	1.05	2.62
3I6Z	1.98	4.22	3.17	2.66	4.05	0.9	1.59	2.47	1.6	4.02	3.31	0.65	0.85	4.16	2.55
1VOT	1.89	3.75	2.58	2.01	3.56	4.96	2.91	2.67	2.14	3.72	4.1	6.48	3.22	1.9	3.28
1E3Q	2.33	4.07	3.75	2.12	3.97	2.74	3.71	1.53	2.29	3.55	3.67	3.45	4.67	2.56	3.17
1OCE	2.72	4.16	3.64	2.63	4.03	2.43	3.09	2.77	2.81	4.02	1.98	0.85	4.13	3.43	3.05
1EVE	2.49	4.03	3.25	3.25	4.27	1.85	1.69	2.91	0.88	4.05	1.99	1	1.31	1.17	2.44
1E66	1.32	2.98	2.68	1.57	5.52	4.84	3.3	2.71	2.68	0.35	5.33	3.86	3.58	0.9	2.97
1W4L	2.12	4.07	3.63	2.29	3.74	0.82	1.7	2.72	1.63	4.03	3.66	0.63	0.86	0.86	2.34
2W6C	1.62	4.3	3.74	2.99	4.3	0.64	1.57	3.01	1.55	3.5	1.28	1.2	1.29	2.07	2.36
1DX6	3.66	3.79	3.55	2.19	4.09	0.84	1.68	2.97	1.16	4.05	3.01	0.76	0.9	3.98	2.62
1W6R	2.72	4.11	3.35	2.5	1.15	0.97	1.71	2.75	1.92	3.84	1.73	0.27	0.54	1.89	2.10
1GPK	2.7	4.14	3.95	2.57	3.29	4.72	2.96	2.9	4.42	3.91	5.77	2.9	3.17	1.72	3.51
2VQ6	2.54	7.43	4.04	1.8	3.41	4.64	3.53	3.2	3.47	10.82	5.13	6.69	6.7	10.22	5.26
3ZV7	3.27	4.27	3.62	2.22	4.12	4.28	1.55	2.89	1.73	4.13	1.62	0.68	0.81	0.83	2.57
1HBJ	2.14	4.66	3	2.29	4.16	5.79	2.91	2.73	2.11	2.51	3.5	4.12	3.24	2.36	3.25
Mean RMSD	2.37	3.67	3.22	2.08	4.01	3.26	2.67	2.73	2.38	3.63	3.01	1.79	1.90	2.21	2.78

Figure 1. The validation of the docking results with RMSD values

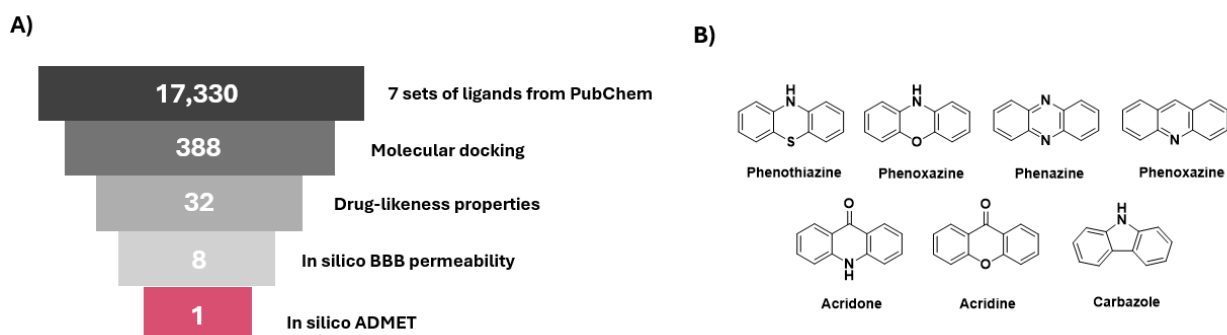


Figure 2. VS workflow (A) and core structure of ligands (B)

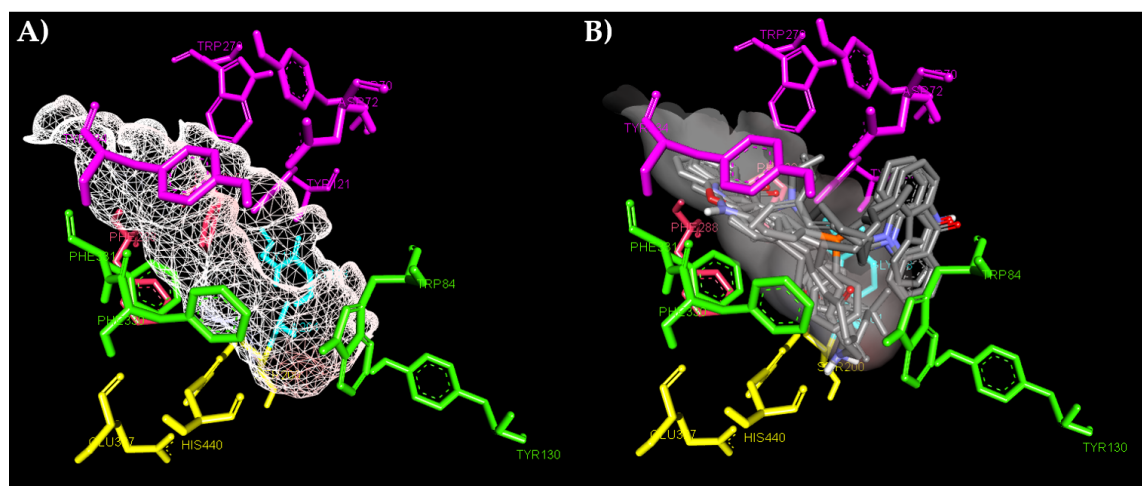


Figure 3. Binding groove of AChE (A) and binding orientation of hits docked into AChE (B). The binding sites are color-coded (catalytic triad; yellow, anionic site; green, peripheral site; purple)

Binding modes of the hit ligands

The active site of AChE is highly specific for ACh, playing a critical role in regulating neuro-transmission. It comprises three key subsites: the catalytic site (CAS), the anionic site (AS), and the peripheral site (PAS). Eight promising ligands were docked into the active site of AChE using

Autodock 4.2.6 software to understand their binding interactions. The AChE binding groove and orientations of these docked ligands within AChE are illustrated in Figure 3. The specific interactions between these ligands and AChE residues are presented in Table 1. When the binding modes were visualized, ligands were in the AChE

Table 1. Structures of Hits, their binding interactions, and binding energies

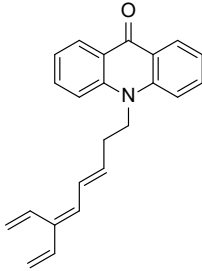
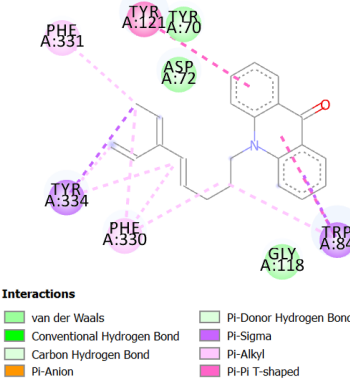
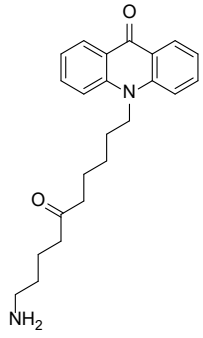
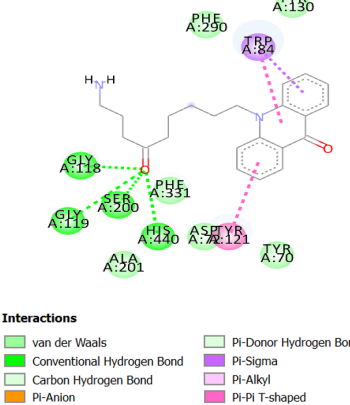
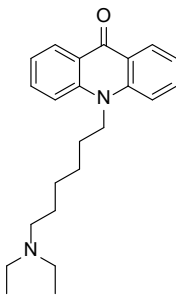
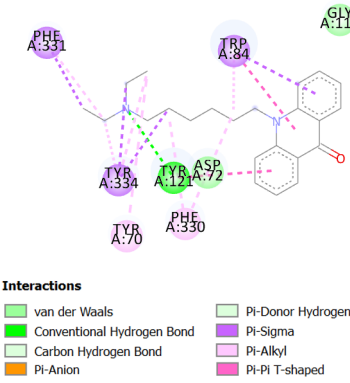
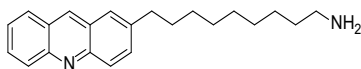
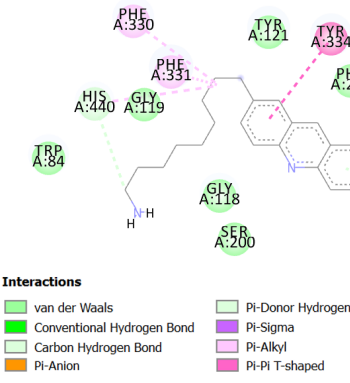
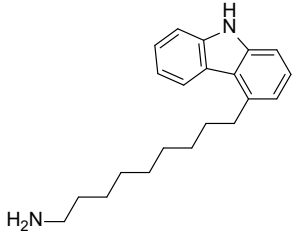
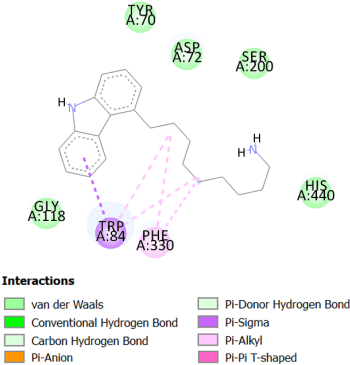
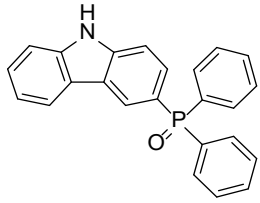
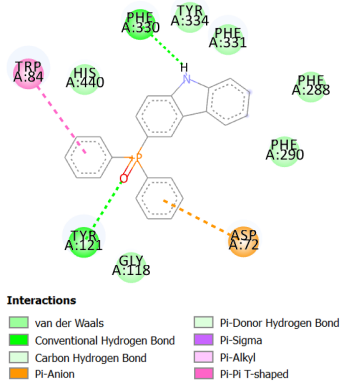
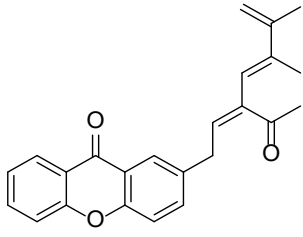
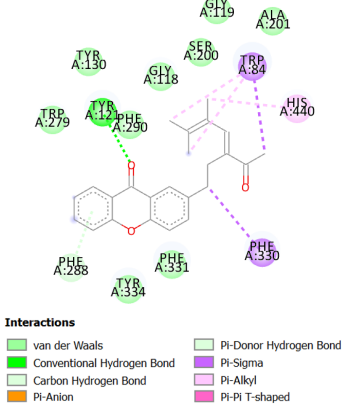
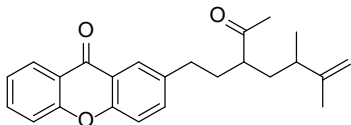
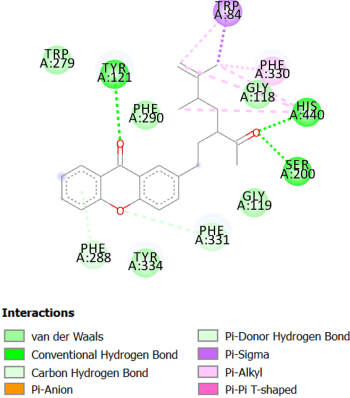
Name/ Structure	Binding interaction	Binding energy (kcal/mol)
(E)-10-(6-vinylocta-3,5,7-trien-1-yl) acridin-9 (10H)-one (M1) 		-10.12
10-(10-amino-6-oxodecyl) acridin-9 (10H)-one (M2) 		-11.71
10-(6-(diethylamino) hexyl) acridin-9 (10H)-one (M3) 		-9.62
9-(acridin-2-yl)nonan-1-amine (M4) 		-11.51

Table 1. Structures of Hits, their binding interactions, and binding energies (continue)

Name/ Structure	Binding interaction	Binding energy (kcal/mol)
9-(9H-carbazol-4-yl) nonan-1-amine (M5) 		-11.52
(9H-carbazol-3-yl) diphenylphosphine oxide (M6) 		-11.31
2-((2Z,4E)-3-acetyl-5,6-dimethylhepta-2,4,6-trien-1-yl)-9H-xanthen-9-one (M7) 		-10.84
2-(3-acetyl-5,6-dimethylhept-6-en-1-yl)-9H-xanthen-9-one (M8) 		-11.15

mid-gorge. The ligands were divided into two groups based on their pose position. The first group consisted of acridones with an aliphatic linker chain at the 10-N position. M6 carbazole was also included in this group due to its binding position. While acridone core structure had a π - π interaction with Trp84 located in AS with their 9-O formed the H-bond with Gly123, its aliphatic linker chain was in CAS. The length of their linker chain at the 10-N position varies with the number of carbons (from 8 to 10). Due to the flexibility of the linker chain, a ketone group in the middle of an M2 linker chain can interact with two amino acids (Ser200 and His440) of the catalytic triad via H-bonds, resulting in its highest binding energy at -11.71 kcal/mol. The linker chains of M1 and M3 were anticipated to interact with Tyr334, Tyr70, and Tyr121 in PAS. Consequently, they were expected to disrupt the acceleration of A β aggregation by AChE. M6 was the only structure with a bulky linker chain. It had the H-bond interaction between 9-NH and Phe330, and two aromatic rings on the linker chain bound to Trp84 and Asp72. The oxygen atom connecting to phosphorus can interact with Tyr121 via the H-bond. The second group belonged to acridine and xanthone, whose core structures were substituted with an aliphatic linker chain at C-7, similar to the first group. M5 carbazole was also in this group because of its binding pose. The acridine binding interaction revealed that the core structure was located near the PAS and bound to Tyr334 via a π - π interaction. The M5 core structure, carbazole, is in the same position as acridine. The NH at C-9 formed interaction with Gln69, and its hydrogen atoms on the linker chain bound to Glu199 through H-bonds. However, one aromatic ring of carbazole can form a π -sigma bond with Trp84. Both ketones at C-9 of xanthone formed an H-bond with Tyr121 at PAS, and their linker chains formed π -sigma interactions with Trp84. The difference between their linker chains was that M7 had a double bond in the middle of the chain, which may reduce its flexibility. Thus, both the oxygen atoms on the linker chain showed different interactions because M8 had more flexibility, supporting that the oxygen atom can form H-bonds with His440 and Ser200.

Drug-likeness and pharmacokinetic properties

To assess the drug-likeness of the eight most promising candidates, their key molecular descrip-

tors were calculated and summarized in Table 2 using the SwissADME. Additionally, the pharmacokinetic properties of the selected ligands were investigated using pKCSM, and the results are presented in Table 3. Ligands have a molecular weight in the range of 308-367 which might easily be transported, diffused, and absorbed. The number of hydrogen bond acceptors and donors were both determined following Lipinski's rule and ranged between 1-2 and 1-3, respectively. Lipophilicity (log P) and topological polar surface area (TPSA) values are two important parameters for predicting oral drug bioavailability. Analysis of the data revealed log P values ranging from 2.41 to 4.29, indicating good cell membrane permeability for these ligands. TPSA is a useful tool both for predicting the oral bioavailability of drug candidates and for optimizing their chemical structures to improve their intestinal absorption. Drugs with TPSA values above 140 Å² tend to be more polar and less likely to cross cell membranes, including the intestinal wall, which can limit their absorption into the bloodstream. As our ligands had ≤ 10 rotatable bonds and TPSA of ≤ 140 Å, they were more likely to have good intestinal absorption, in the range of 95-100%. Additionally, all these ligands showed good distribution values of more than -2, indicating their potential to penetrate the CNS. Moreover, M1 and M3 had values greater than 0.3, indicating their ability to cross the BBB and that the remaining ligands could also pass through it. In metabolism, some hits are susceptible to biotransformation by the CYP450 enzyme system. However, M8 was found to be a substrate of P-glycoprotein, which effluxes drugs and other substances for further metabolism and clearance. However, none of the ligands were found to be OCT2 substrates, which can induce nephrotoxicity by changing drug accumulation in the kidney. Only M5 was found to be unlikely to cause hepatotoxicity.

Molecular dynamics simulations

Molecular dynamics simulations were used to assess the structural stability, flexibility, and compactness of the M5-AChE complex. The M5-AChE complex was compared to a native enzyme (apo) and donepezil-AChE complex (donepezil) in terms of various parameters including RMSD, RMSF, and RoG analysis. Our results showed that RMSD between apo, standard, and M5 are in

Table 2. Physicochemical properties of hits predicted by the SwissADME program.

Molecule	MW	Rotatable bonds	H-bond acceptors	H-bond donors	TPSA	MLOGP
M1	327.42	6	1	0	22.00	4.14
M2	350.45	9	3	1	65.09	2.41
M3	350.50	9	2	0	25.24	3.55
M4	320.47	9	2	1	38.91	4.29
M5	308.46	9	1	2	41.81	4.11
M6	367.38	3	1	1	42.67	4.25
M7	358.43	5	3	0	47.28	3.47
M8	362.46	7	3	0	47.28	3.61

MW, molecular weight; TPSA, Topological polar surface area

Table 3. Pharmacokinetic properties of hits predicted by pKCSM program.

ADMET	Parameters	Acridone			Acridine	Carbazole		Xanthone	
		M1	M2	M3	M4	M5	M6	M7	M8
Absorption	Caco2 permeability	1.054	0.53	1.029	1.225	1.399	0.894	1.079	1.119
Absorption	Intestinal absorption (human)	97.622	98.1	95.352	94.412	91.142	100	98.36	98.488
Distribution	VDss (human)	0.738	1.021	1.667	1.376	1.208	-1.123	0.176	0.418
Distribution	BBB permeability	0.703	-0.425	0.786	-0.083	-0.164	-0.027	-0.241	-0.294
Distribution	CNS permeability	-1.263	-2.448	-1.536	-1.639	-1.957	-1.275	-1.338	-1.453
Metabolism	CYP2D6 substrate	No	No	Yes	No	No	No	No	No
Metabolism	CYP3A4 substrate	Yes	Yes	Yes	Yes	Yes	Yes	Yes	Yes
Metabolism	CYP1A2 inhibitor	Yes	Yes	Yes	Yes	Yes	Yes	Yes	Yes
Metabolism	CYP2C19 inhibitor	Yes	No	Yes	No	Yes	Yes	Yes	Yes
Metabolism	CYP2C9 inhibitor	Yes	No	No	No	No	No	Yes	Yes
Metabolism	CYP2D6 inhibitor	No	No	Yes	Yes	Yes	Yes	No	No
Metabolism	CYP3A4 inhibitor	No	Yes	Yes	No	No	No	No	No
Excretion	Renal OCT2 substrate	No	No	No	No	No	No	No	No
Toxicity	Hepatotoxicity	Yes	Yes	Yes	Yes	No	Yes	Yes	Yes

ADMET stands for absorption, distribution, metabolism, elimination, and toxicity

the range of 0.59 to 1.77 Å throughout the 50 ns which is within the acceptable range (1–3 Å) (Figure 4A). The average RMSD of apo, donepezil, and M5 were 1.31 ± 0.17 , 1.34 ± 0.14 , and 1.39 ± 0.16 Å, respectively. However, the flexibility pattern of M5 was similar to apo and donepezil, except regions 70–80 and 420–450 (Figure 4B). The mean RMSF value of AChE–M5 complex was determined to be 0.74 Å. The average RoG of apo, donepezil and M5 were 22.79, 22.86 and 22.83 Å,

respectively (Figure 4C). There was no significant deviation observed and compactness was maintained throughout the trajectory.

Identification of potential anti-AD targets and protein-protein interaction (PPI) network analysis

SwissTargetPrediction identified 107 potential targets of M5. Subsequently, 13,564 targets associated with AD were retrieved from GeneCards.

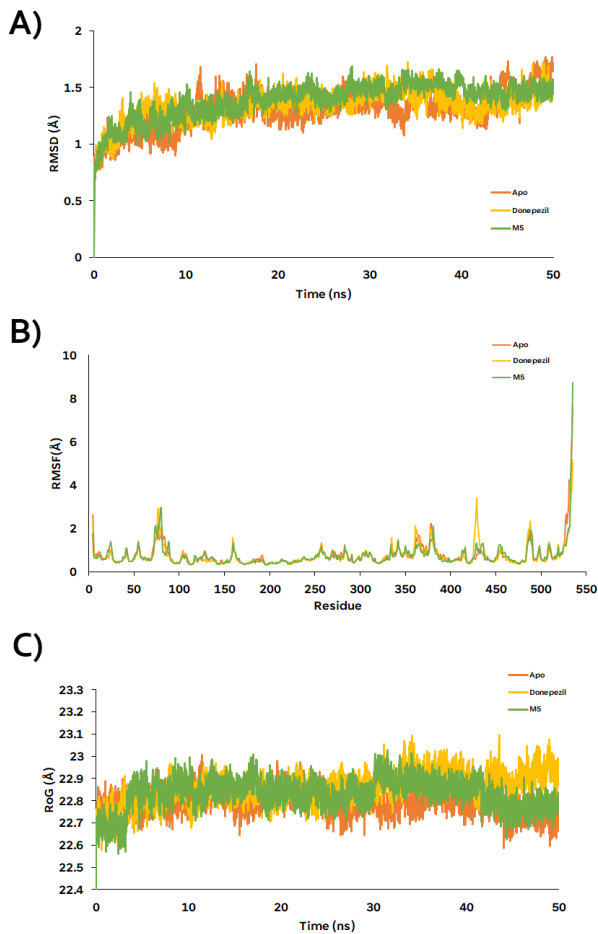


Figure 4. Molecular dynamics analysis: RMSD (A), RMSF (B), RoG (C)

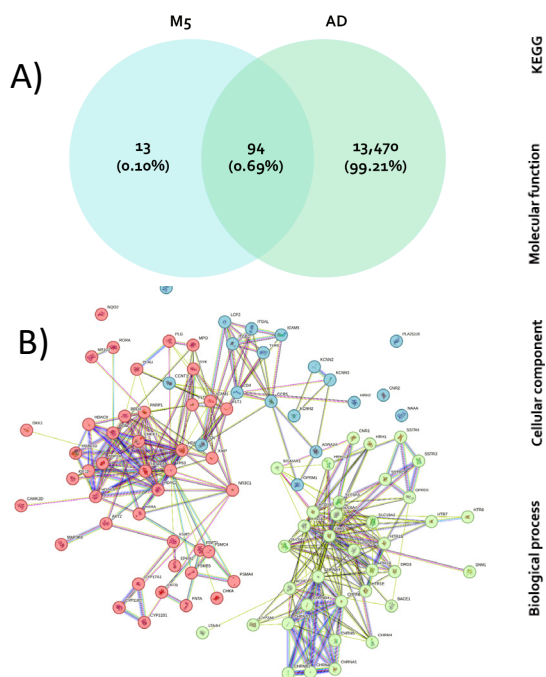


Figure 5. Shared targets represented in a Venn diagram (A), the top three cluster subnetworks (B), GO and KEGG function analysis (C)

A Venn diagram (Figure 5A) was created to visualize the overlap between these M5-related and AD-related genes, resulting in the identification of 94 potential anti-AD target genes of M5. To further explore the interactions between these 94 targets, a PPI network was constructed using the STRING database (Figure 5B). This network provides a comprehensive view of the molecular associations relevant to M5 and AD.

Functional enrichment analysis of M5 targets

GO and KEGG pathway enrichment analyses were performed to understand the functions and pathways associated with M5 targets. The targets were significantly enriched ($p < 0.05$) in 665 GO terms, with a breakdown of 527 for biological processes (BP), 55 for cellular components (CC), and 83 for molecular functions (MF). The top 10 most enriched GO terms are visualized in Figure 5C. The response to the chemical (GO:0042221) in BP is the process which resulted in a change in cell activity via chemical stimulation. CC is prominently engaged as an integral component of plasma membrane (GO:0005886) and neuron projection (GO:0043005). The MF analysis highlighted involvement in neurotransmitter receptor activity (GO:0030594) and signaling receptor activity (GO:0038023).

KEGG pathway analysis

To further validate that these enriched biological processes are relevant to AD, KEGG pathway analysis was used to identify significantly enriched pathways ($p < 0.05$) associated with the target genes (Figure 5C). KEGG pathway analysis constitutes a valuable tool for augmenting comprehension of the biological functions attributed to genes. The investigation of M5 targets through the KEGG pathway unveiled noteworthy enrichment within neuroactive ligand-receptor interaction (hsa04080).

Analysis of gene clusters for key genes

To clarify the effects of M5 on AD, we identified the top three clusters with high scores and closely interconnected regions from the PPI network (Figure 5B). These clusters, containing 43 (red), 36 (green), and 19 (blue) genes (Table 4), represent potential key players and their interactions in the context of M5 and AD. Analyzing these gene clusters can aid in identifying key genes and their interactions. The clusters retrieved from the String-db and kmeans clustering algorithm was applied to the gene correlation. The major pathways of the clusters were selected and are represented in Figure 6. Cluster 1 demonstrated a predominant involvement in neutrophil extracellular trap (NET) formation and viral carcinogenesis. Cluster 2 was associated with neuroactive ligand-receptor interaction, and Cluster 3 was engaged in natural killer (NK) cell-mediated cytotoxicity and the modulation of cell adhesion molecules.

DISCUSSION

This study employed a virtual screening (VS) approach to identify potential drug candidates for Alzheimer's disease (AD). We focused on targeting acetylcholinesterase (AChE), a key enzyme implicated in AD pathogenesis. Following virtual screening, *in silico* docking simulations were used to predict and confirm binding interactions of identified hits with AChE. Finally, network pharmacology was utilized to explore the potential mechanisms by which these promising candidates might exert their effects on AD.

Public databases like PubChem offer a wealth of chemical structures, but raw data can be incomplete and poorly understood, leading to unstructured data concerns (17–19). Tacrine, a simple AChEI fragment, suffers from hepatotoxicity, highlighting the need for alternative scaffolds (20). AChE binding pocket is known to comprise a hydrophobic pocket, which is ideally suited for planar aromatic molecules. A total of seven classes of such ligands were chosen for VS and docking simulations. Donepezil's high selectivity for AChE supports the cholinergic hypothesis, and ligands scoring higher were considered promising candidates (21). Drug-likeness and blood-brain barrier (BBB) permeability filters were applied to prioritize suitable chemical candidates. Orally active drugs reaching phase II clinical trials often adhere to Lipinski's rule. Additionally, BBB permeability is crucial for CNS drugs due to restricted passage: only lipophilic molecules with low molecular weight (typically below 400–500 Da) can pass through the BBB (22).

Table 4. The clusters of the most interlinked regions

Bubble	Cluster	Gene count	Protein names
Red	1	43	AKT2, BRD4, CAMK2D, CHEK1, CHKA, CYP11B1, CYP11B2, CYP17A1, DKK1, EPHX2, ESR2, FDFT1, FLT1, FLT3, FNTA, FNTB, HDAC1, HDAC10, HDAC2, HDAC3, HDAC4, HDAC5, HDAC6, HDAC9, ICAM1, KIF11, MAP3K8, MPO, NQO2, NR1D2, NR3C1, PARP1, PLA2, PLG, PSMA4, PSMB5, PSMC4, RORA, RXRA, SYK, TOP2A, TP53, XIAP
Green	2	36	ACHE, BACE1, CHRM4, CHRM5, CHRNA1, CHRNA3, CHRNA4, CHRNA7, CHRNB1, CHRNB2, CHRNB4, CNR1, CYP2A6, DNM1, DRD2, DRD3, HRH1, HRH3, HTR1A, HTR1B, HTR1D, HTR1E, HTR2A, HTR2C, HTR6, HTR7, LTA4H, OPRD1, SIGMAR1, SLC18A2, SLC6A2, SLC6A3, SLC6A4, SSTR2, SSTR3, SSTR4
Blue	3	19	ADRA2A, CCNT1, CCR5, CD4, CNR2, HRH2, ICAM3, ITGAL, ITGB2, KCNH2, KCNN2, KCNN3, LCK, LCP2, NAAA, OPRM1, PIM2, PLA2G1B, TLR8

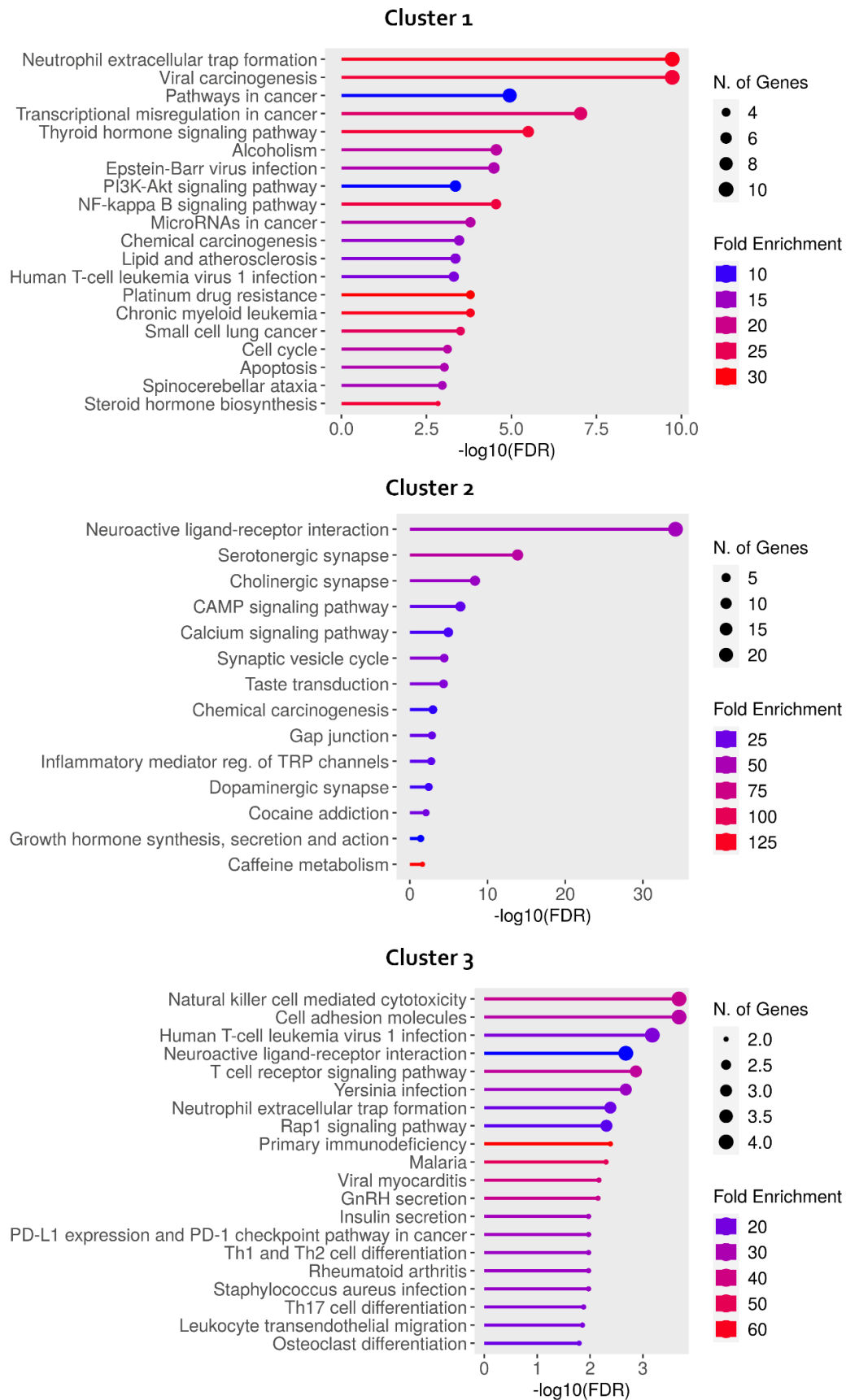


Figure 6. KEGG pathway enrichment analysis of key targets after clustering

Our analysis categorized the identified hits into two distinct groups based on their binding pose within the AChE active site. In group 1 (acridones), these ligands primarily reside near the anionic site. They interact with Trp84, a critical amino acid responsible for binding the quaternary ammonium group of ACh and ensuring its proper positioning for hydrolysis (23). This interaction suggests group 1 ligands may act as acetylcholinesterase inhibitors by competitively blocking or interfering with this crucial step. Additionally, their binding to Gly118 and Gly119 in the oxyanion hole near CAS could significantly impact ACh hydrolysis by destabilizing the transition state, likely leading to potent inhibition (23). For group 2 (acridine, xanthone, and carbazole (M5)), the binding orientation of this group suggests potential interaction with both the PAS and the CAS. While they may establish hydrogen bonds within the CAS, potentially influencing ACh hydrolysis, their primary location near the PAS suggests a possible role in interfering with A β aggregation.

Poor pharmacokinetics and pharmacodynamics features are the main causes of the clinical failure and limitations of many drug candidates. The permeability of the CNS refers to a substance's ability to cross the membranes that surround and protect the brain, spinal cord, and cerebrospinal fluid (24). The BBB permeability is critical in determining the efficacy and safety of drugs targeting the CNS. The BBB acts as a specialized barrier that regulates the entry of drugs and other substances into the brain (24). CYP1A2, CYP2A6, CYP2C9, CYP2C19, CYP2D6, CYP2E1, and CYP3A4 are the significant isoforms of the cytochrome P450 (CYP450) family which is involved in drug metabolism and clearance (25). The disturbance of CYP450 metabolism can lead to altered pharmacokinetics, such as reduced bioavailability or increased clearance, which may affect the efficacy of the drug. Furthermore, drug-drug interactions can occur when a drug candidate alters the activity of CYP450 enzymes, resulting in changes in the metabolism of co-administered drugs and potentially leading to adverse effects (26, 27). All candidates showed favorable pharmacokinetic profiles with the exception of hepatotoxicity. This might be because of their structures as the pkCSM webserver was built using the liver-associated side effects of compounds observed in humans in

their database. It is important to note that hepatotoxicity caused by drugs is rare and unpredictable. Nevertheless, *in vitro* and *in vivo* studies are required to observe their effects further.

Through the VS approach, M5 was identified as a promising ligand, exhibiting lower binding energy compared to a current standard AD drug donepezil, along with having favorable predicted pharmacokinetic profiles. Moreover, it showed a similar pharmacophore feature, containing one hydrogen bond acceptor, two hydrogen bond donors, one aromatic ring and one hydrophobic center, which is consistent with a hit in a previous study (28).

MD simulations were used to further explore the interaction and stability of M5 with AChE. The RMSD was used to assess the fluctuation in system stability and to determine the time point at which the system achieved equilibrium. After 20 ns, the complex reached equilibrium with slight fluctuations, exhibiting stable binding between ligand and enzyme. On the other hand, the RMSF was calculated to study the protein flexibility with the ligand binding, providing insight into changes in conformation. High fluctuations occurred at regions 70–80 and 420–450 which correspond to the PAS and CAS regions. There was a significant fluctuation observed near His440 which indicates that M5 had more stable interaction than donepezil, a current benchmark treatment. This supports that M5 can bind with both CAS and PAS regions.

Network pharmacology was employed to delineate its underlying mechanisms in AD. Through this analysis, ninety-four overlapping genes were identified, and subsequently an interaction network was constructed to explore the core regulatory genes. GO enrichment analysis is instrumental in providing information for understanding the diverse roles that genes play in various biological contexts (29). BP is particularly relevant to the changes in the biological functions, and it can provide insights into the specific activities or events involving genes that contribute to the overall functioning of a cell. CC aspect focuses on identifying the specific parts of a cell or its extracellular environment where a gene product is located while MF describes the specific biochemical activity performed by the gene product. Our findings regarding the functional characteristics of M5 indicate it might bind to the target protein and

exert a sophisticated network of interactions. The chemical signals, recognized by receptors in the integral component of the plasma membrane, initiate signaling cascades that influence neuron projections and neurotransmitter receptor activity (30–32). Understanding this response is crucial for unraveling the complex mechanisms underlying neural communication and cellular function. KEGG analysis was used to better explain the mechanism of M5 at the pathway level. The neuroactive ligand-receptor interaction pathway serves as a critical framework for understanding the complexities of synaptic transmission, neuromodulation, and the control of neuronal excitability. That pathway includes various neuroactive ligands, such as neurotransmitters, hormones, and other signaling molecules, that play crucial roles in neuronal signaling (33). AD involves complex molecular mechanisms which might be associated with the neuroactive ligand-receptor interaction pathway. This pathway is interconnected with several pathways, such as those related to cholinergic deficiency, glutamate dysregulation, inflammation, oxidative stress, and cell death. The crosstalk between these pathways contributes to the multifaceted nature of AD.

Clustering represents the links between genes, corresponding to gene interaction relationships. Three clusters were speculated to play roles in M5 treated AD. Cluster 1 is enriched for genes involved in neutrophil extracellular trap (NET) formation. NET formation has been linked to chronic neuroinflammation, a hallmark of AD pathology. Additionally, activated neutrophils contribute to inflammation by triggering MMP-9, an enzyme associated with BBB disruption (34–39). This suggests that M5 might target NET formation and BBB integrity, potentially reducing neuroinflammation. Cluster 2 focused on neuroactive ligand-receptor interactions. These interactions influence neuronal function and gene expression. Genetic disruptions in these pathways are known to impair memory function (40). M5's influence on this cluster suggests a potential role in memory preservation. Cluster 3 is associated with natural killer (NK) cell activity and cell adhesion. NK cells eliminate abnormal cells, including those linked to inflammation (41). Cell adhesion molecules facilitate communication between immune cells which is crucial for effective immune responses

(42). Dysfunctional NK cells and dysregulated immune responses are observed in AD (43–45). M5's impact on this cluster indicates a potential role in enhancing NK cell function and immune response regulation. These findings suggest M5 might exert anti-AD effects through multiple molecular targets beyond just AChE inhibition. The clustering analysis points towards neuroinflammation as a potentially key target for M5's action against AD. However, it is important to acknowledge the limitations of this study: the proposed mechanisms are theoretically supported, but further research is needed for confirmation.

Overall, this virtual screening study identified M5 as a promising lead compound for Alzheimer's disease with a predicted binding affinity stronger than donepezil, a current standard treatment. M5 exhibited favorable pharmacokinetic properties and interacted stably with both the catalytic site and peripheral anionic site of acetylcholinesterase in molecular docking simulations. Network pharmacology analysis suggested M5 might target multiple pathways implicated in Alzheimer's disease, potentially through its interaction with neuroactive ligand-receptor interactions and modulation of inflammatory responses. While this study provides a promising starting point for drug development, further validation is needed. *In vitro* and *in vivo* experiments are required to confirm the identified hits and their mechanisms of action. Additionally, the potential hepatotoxicity of M5 needs investigation. Addressing these limitations could potentially translate these *in silico* findings into a robust pre-clinical development plan for M5 as a potential therapeutic candidate for AD.

CONCLUSIONS

Our VS identified promising ligands predominantly from three scaffolds: acridone, carbazole, and xanthone. Docking simulations demonstrated their strong binding affinity and stability within the active site of enzymes. These ligands, characterized by an aromatic core structure, interacted effectively with key amino acids, potentially disrupting ACh hydrolysis. These ligands were in an active site, preventing ACh from accessing the CAS, thus potentially inhibiting AChE activity more effectively. To optimize binding, extending the linker chain to enhance hydrophobic interac-

tions is crucial. Incorporating an electron-withdrawing group, such as a ketone, in the linker chain can further enhance binding affinity. The *in silico* pharmacokinetic properties were investigated, and ligands were found to exhibit several favorable pharmacokinetic properties. M5 was the only ligand that did not exhibit hepatotoxicity, suggesting it may present a lower risk of causing liver damage compared to others. MD simulations explored the interaction and stability of M5 with AChE, comparing it with native complexes and the donepezil-AChE complex. Results showed that M5 bound stably, potentially engaging both CAS and PAS regions, suggesting it might act as dual-binding AChE inhibitor. Compared to donepezil, M5 showed potentially more favorable interactions, particularly near His440, indicating unique binding characteristics. In addition, network analysis found that M5 might exert anti-AD effects through multiple molecular targets, extending beyond AChE inhibition. Clustering analysis hinted at a potential focus on neuroinflammation in the M5 mechanism of action against AD. Additional experimental validation *in vitro* and *in vivo* is necessary for advancing M5 towards clinical application.

ACKNOWLEDGMENTS

None

FUNDING

This research was supported by the Fundamental Fund of Khon Kaen University under the National Science, Research and Innovation Fund; Khon Kaen University under Grant number 631JH218; Faculty of Pharmaceutical Sciences, Khon Kaen University; Visiting Professor Scholar under BCG Economy and Sustainable Development Network through the Center of Excellence Consortium, Khon Kaen University; Fulbright-2022 Junior Research Scholarship Program; and Ubon Ratchatani University, Thailand.

CONFLICTS OF INTEREST

The authors declare no conflict of interest.

ADDITIONAL INFORMATION

Author contributions

Conceptualization, C.B., P.W., Y.C. and C.Ba.; methodology, P.T., C.B., P.W.; software, P.T., K.C.,

C.B.; formal analysis, P.T., C.B., P.W.; investigation, P.T., C.B., P.W. P.A.; resources, C.B.; writing—original draft preparation, P.T., and C.B.; writing—review and editing, C.B., and P.W.; project administration, C.B. All authors have read and agreed to the published version of the manuscript.

Data availability statement

Data is contained within the article.

Institutional review board statement

Not applicable

Informed consent statement

Not applicable

REFERENCES

1. United Nations, Department of Economic and Social Affairs, Population Division. World population ageing 2019: Highlights. New York: United Nations; 2019.
2. Hasselmo M. The Role of acetylcholine in learning and memory. *Curr Opin Neurobiol*. 2006;16:710-5.
3. Chen Z, Huang J, Yang S, Hong F. Role of cholinergic signaling in Alzheimer's disease. *Molecules*. 2022;27:1816. PubMed PMID: 35335180
4. Giacobini E. Is anti-cholinesterase therapy of Alzheimer's disease delaying progression? *Aging (Milano)*. 2001;13:247-54.
5. Čolović M, Krstić D, Lazarević-Pašti T, Bondžić A, Vasić V. Acetylcholinesterase inhibitors: pharmacology and toxicology. *Curr Neuropharmacol*. 2013;11:315-35.
6. Budd Haeberlein S, Aisen P, Barkhof F, Chalkias S, Chen T, Cohen S, et al. Two randomized phase 3 studies of aducanumab in early Alzheimer's disease. *J Prev Alzheimers Dis*. 2022;9:197-210.
7. Kapetanovic I. Computer-aided drug discovery and development (CADD): *in silico*-chemico-biological approach. *Chem Biol Interact*. 2008;171:165-76.
8. Mohs R, Greig N. Drug discovery and development: role of basic biological research. *Alzheimers Dement (N Y)*. 2017;3:651-7.
9. Muegge I, Oloff S. Advances in virtual screening. *Drug Discovery Today: Technologies*. 2006;3:405-11.
10. Wu F, Zhou Y, Li L, Shen X, Chen G, Wang X, Liang X, Tan M, Huang Z. Computational approaches in pre-clinical studies on drug discovery and development. *Front Chem*. 2020;8:726. PubMed PMID: 33062633.
11. Durrant J, McCammon J. Molecular dynamics simulations and drug discovery. *BMC Biology*. 2011;9:71. PubMed PMID: 22035460.
12. Daina A, Michielin O, Zoete V. SwissADME: a free web tool to evaluate pharmacokinetics, drug-likeness and medicinal chemistry friendliness of small molecules. *Sci Rep*. 2017;7:42717. PubMed PMID: 28256516.
13. Pires D, Blundell T, Ascher D. pkCSM: predicting small-molecule pharmacokinetic and toxicity prop-

- erties using graph-based signatures. *J Med Chem.* 2015;58:4066–72.
14. Eastman P, Swails J, Chodera J, McGibbon R, Zhao Y, Beauchamp K, et al. OpenMM 7: rapid development of high performance algorithms for molecular dynamics. *PLoS Comput Biol.* 2017;13:e1005659. PubMed PMID: 28746339.
 15. Tian C, Kasavajhala K, Belfon K, Raguette L, Huang H, Migués A, et al. ff19SB: amino-acid-specific protein backbone parameters trained against quantum mechanics energy surfaces in solution. *J Chem Theory Comput.* 2020;16:528–52.
 16. Lipinski C, Lombardo F, Dominy B, Feeney P. Experimental and computational approaches to estimate solubility and permeability in drug discovery and development settings. *Adv Drug Deliv Rev.* 2001;46:3–26.
 17. Tiikkainen P, Franke L. Analysis of commercial and public bioactivity databases. *J Chem Inf Model.* 2012;52:319–26.
 18. Tetko I, Engkvist O, Koch U, Reymond J, Chen H. BIGCHEM: challenges and opportunities for big data analysis in chemistry. *Molecular Informatics.* 2016;35:615–21.
 19. Kim S, Thiessen PA, Bolton EE, Chen J, Fu G, Gindulyte A, et al. PubChem substance and compound databases. *Nucleic Acids Res.* 2016;44(Database issue):D1202–13.
 20. Marucci G, Buccioni M, Ben D, Lambertucci C, Volpini R, Amenta F. Efficacy of acetylcholinesterase inhibitors in Alzheimer's disease. *Neuropharmacology.* 2021;190:108352. PubMed PMID: 33035532.
 21. Ogura H, Kosasa T, Kuriya Y, Yamanishi Y. Comparison of inhibitory activities of donepezil and other cholinesterase inhibitors on acetylcholinesterase and butyrylcholinesterase *in vitro*. *Methods Find Exp Clin Pharmacol.* 2000;22:609–13.
 22. Khawli LA, Prabhu S. Drug delivery across the blood-brain barrier. *Mol Pharmaceutics.* 2013;10:1471–2.
 23. Bajda M, Więckowska A, Hebda M, Guźior N, Sotriuffer C, Malawska B. Structure-based search for new inhibitors of cholinesterases. *IJMS.* 2013;14:5608–32.
 24. Kadry H, Noorani B, Cucullo L. A blood-brain barrier overview on structure, function, impairment, and biomarkers of integrity. *Fluids Barriers CNS.* 2020;17:69. PubMed PMID: 33208141.
 25. Zanger U, Schwab M. Cytochrome P450 enzymes in drug metabolism: regulation of gene expression, enzyme activities, and impact of genetic variation. *Pharmacol Ther.* 2013;138:103–41.
 26. Bhatia S. Concise guide to drug interaction principles of medical practice: cytochrome P450s, UGTs, P-Glycoproteins, Second Edition. *J Am Acad Child Adolesc Psychiatry.* 2005;44:607–8.
 27. Lynch T, Price A. The effect of cytochrome P450 metabolism on drug response, interactions, and adverse effects. *Am Fam Physician.* 2007;76:391–6.
 28. Gade AC, Murahari M, Pavada P, Kumar MS. Virtual screening of a marine natural product database for *in silico* identification of a potential acetylcholinesterase inhibitor. *Life.* 2023;13:1298. PubMed PMID: 37374081.
 29. Thomas PD. The gene ontology and the meaning of biological function. *Methods Mol Biol.* 2017;1446:15–24.
 30. Cooper GM. Structure of the plasma membrane. In: *the cell: a molecular approach* 2nd edition [Internet]. Sinauer Associates; 2000 [cited 2024 Jan 25]. Available from: <https://www.ncbi.nlm.nih.gov/books/NBK9898/>
 31. Ray S, Kassan A, Busija A, Rangamani P, Patel H. The plasma membrane as a capacitor for energy and metabolism. *Am J Physiol Cell Physiol.* 2016;310:C181–92.
 32. Cho I, Jackson M, Swift J. Roles of cross-membrane transport and signaling in the maintenance of cellular homeostasis. *Cell Mol Bioeng.* 2016;9:234–46.
 33. Lauss M, Kriegner A, Vierlinger K, Noehammer C. Characterization of the drugged human genome. *Pharmacogenomics.* 2007;8:1063–73.
 34. DeTure M, Dickson D. The neuropathological diagnosis of Alzheimer's disease. *Mol Neurodegener.* 2019;14:32. PubMed PMID: 31375134.
 35. Kinney J, Bemiller S, Murtishaw A, Leisgang A, Salazar A, Lamb B. Inflammation as a central mechanism in Alzheimer's disease. *Alzheimers Dement (N Y).* 2018;4:575–90.
 36. Pietronigro E, Della Bianca V, Zenaro E, Constantin G. NETosis in Alzheimer's disease. *Front Immunol.* 2017;8:211. PubMed PMID: 28303140.
 37. Turner R, Sharp F. Implications of MMP9 for blood brain barrier disruption and hemorrhagic transformation following ischemic stroke. *Front Cell Neurosci.* 2016;10:56. PubMed PMID: 26973468.
 38. Chen Y, Williams V, Filippova M, Filippov V, Duerksen-Hughes P. Viral carcinogenesis: factors inducing dna damage and virus integration. *Cancers (Basel).* 2014;6:2155–86.
 39. Pezone A, Olivieri F, Napoli MV, Procopio A, Avvedimento EV, Gabrielli A. Inflammation and DNA damage: cause, effect or both. *Nat Rev Rheumatol.* 2023;19:200–11.
 40. Papassotiropoulos A, de Quervain D. Failed drug discovery in psychiatry: time for human genome-guided solutions. *Trends Cogn Sci.* 2015;19:183–7.
 41. Zitti B, Bryceson Y. Natural killer cells in inflammation and autoimmunity. *Cytokine Growth Factor Rev.* 2018;42:37–46.
 42. Harjunpää H, Lloret Asens M, Guenther C, Fagerholm S. Cell adhesion molecules and their roles and regulation in the immune and tumor microenvironment. *Front Immunol.* 2019;10:1078. PubMed PMID: 31231358.
 43. Sharma P, Kumar P, Sharma R. Natural killer cells - their role in tumour immunosurveillance. *J Clin Diagn Res.* 2017;11:BE01–5.
 44. Qi C, Liu Q. Natural killer cells in aging and age-related diseases. *Neurobiol Dis.* 2023;183:106156. PubMed PMID: 37209924
 45. Baechle JJ, Chen N, Makhijani P, Winer S, Furman D, Winer DA. Chronic inflammation and the hallmarks of aging. *Mol Metab.* 2023;74:101755. PubMed PMID: 37329949